Proceedings of the 28th IEEE
EMBS Annual International Conference
New York City, USA, Aug 30-Sept 3, 2006



# LMS-based Active Noise Cancellation Methods for fMRI Using Sub-band Filtering

Ali A. Milani, *Student Member*. Issa Panahi, Richard Briggs, *Member, IEEE*

*Abstract*— **We present application of adaptive LMS-based method using two different sub-band filtering techniques for active reduction of 3T-fMRI acoustic noise. Analysis and design of the sub-band filters are discussed based on the characteristics of the noise. Using the fMRI-Brain scanner acoustic noise, performance of the methods are analyzed and compared for different number of sub-band filters.**

## I. INTRODUCTION

In modern high magnetic field (more than 3 Tesla) fMRI scanners, the gradient acoustic noise produced by switching the gradient current reaches to more than 130 dB SPL. Such laud sound is not only intolerable for the patient undergoing the examination, but also is a major interference to the audio communication with the patient. The presence of the scanner noise may also deleteriously affect fMRI experiments in which it is desired to stimulate the auditory regions of the brain, thus reducing the dynamic range available for activation by the stimulus of interest [1]. Even in fMRI experiments not focused on studying the brain's perception of sound, e.g., in studies of word generation, it is often useful to present the auditory stimulus cues. Because of this, the reduction of acoustic noise and the enhancement of the recorded speech quality during scanning are of great interest in conducting advanced fMRI experiments.

Echo planar imaging (EPI) sequences are usually used for fMRI, because acquisition of images, typically 20 to 40 two-dimensional slices, for the entire brain volume can be obtained rapidly in 1 to 3 seconds. The spectral characteristics and amplitude of the acoustic noise depend on the design of the magnet and gradient coils and on the switching sequence used to operate the scanner. The amplitude of the noise is proportional to the strength of the magnetic field present in the scanner [3]. Figure 1(a) shows the recorded 3T MRI acoustic noise signal during a typical EPI sequence and Figure 1(b) shows its spectrum. Several techniques, mainly based on passive and active noise control (ANC), are commonly employed to reduce this background noise. Use of earplugs, ear defenders, and sound-absorbing foam lining in the magnet bore are some types of passive methods that are used to suppress the fMRI noise up to about 40 dB. However, these methods generally do not work well for the low-frequency part of the noise, which has a large wavelength compared to the thickness of a typical acoustic noise absorber [2]. To obtain an efficient real-time ANC system for the wideband fMRI-scanner noise, we divide the spectrum of the noise signal into a number of sub-bands in frequency domain and apply a normalized LMS-based FIR filter of lower length for each sub-band. Finally the main noise canceling filter weights for the ANC system are constructed from the weights of every sub-band LMS filters. Morgan [6] introduced a novel delay-less sub-band filtering architecture. But the frequency response of its synthesis filters has deep nulls in the pass-bands (Figure 5). This is not suitable for our design case, where the spectrum of the fMRI acoustic noise has strong tonal components. We have modified the weight stacking method in Morgan's architecture to avoid losing these tonal components. We also show the dependency of the noise reduction on the number of sub-bands and the acoustic noise characteristics. This has led us to choose an optimal sub-band filtering scheme which offers high attenuation of the acoustic noise for a 3T fMRI scanner system. Performance and computation burden of the sub-band based methods, for different number of sub-band filters, are compared with the LMS method using no sub-band filtering. In Section II we describe the reasons why the sub-band filtering is chosen. In Section III the methods based on two sub-band filtering techniques are presented. Finally, Section IV presents the simulation results and shows the performance of the proposed method for fMRI acoustic noise reduction.

## II. SUB-BAND FILTERING FOR FMRI NOISE

ANC systems that use LMS or RLS for full-band fMRI adaptive filtering are good at handling low-frequency and narrow-band signals, but need considerably high order FIR filters in order to model the acoustic system accurately. The delay produced by this FIR filter compared to the short distance between microphone and speaker degrades the performance of the system. Furthermore, high-order FIR filters lower the convergence rate and require more computations. In full-band filtering, this can lead to instabilities due to the high ratio of the maximum to minimum singular values of the input correlation matrix. If a

This work is supported by a subcontract from the Epidemiology Division, Department of Internal Medicine, UT Southwestern Medical Center at Dallas under grant no. DAMD17-01-1-0741 from the U.S. Army Medical Research and Materiel Command. The content of this paper does not necessarily reflect the position or the policy of the U.S. government, and no official endorsement should be inferred.

Ali A. Milani is a PhD student at the electrical engineering department of University of Texas at Dallas, Dallas, TX ( e-mail: ali.a.milani@student.utdallas.edu).

Issa Panahi is with the electrical engineering department of University of Texas at Dallas, Dallas, TX (e-mail: issa.panahi@utdallas.edu).

Richard Briggs is with the department of radiology, University of Texas Southwestern Medical Center, Dallas, TX .

notch exists in the secondary path at some frequency, a very small amount of signal will be detected by the error microphone. Consequently, the high-order adaptive filter will not adjust the filter coefficients properly, resulting in small or no cancellation at that frequency. In the case of fMRI, the noise spectrum as shown in Figure 1(b) has strong tonal components between 500 and 2000 Hz, with harmonics of considerable amplitudes. This special characteristic of the noise worsens the performance of the conventional adaptive filtering method and requires a more suitable approach. Due to the noise spectrum and the aforementioned drawbacks associated with full-band adaptive filtering, the sub-band filtering approach is proposed as an alternative solution to the ANC problem.

Figure 2 shows the sub-band filtering used in our implementation of the fMRI ANC system. The reference $x'(n)$ and the error signal $e(n)$ are each filtered into $M$ sub-bands using a uniform filter bank as shown in Figure 2. The LMS algorithm computes the weighting of the filter for each sub-band. The sub-band weights are stacked constructing the $W(n)$ as the main noise canceling filter as discussed in [6-7]. Sub-band filtering allows us to treat a wide-band signal as a set of narrow-band signals. Consequently, the LMS-based adaptive filters work better, because the dynamic range of the input signal is smaller, the ratio of the maximum to minimum singular values of the input correlation matrix is smaller [4], and notches in the input signal can be tracked and handled more easily. An important feature of the sub-band adaptive filtering method lies in its efficient and delays-less implementation [6]. We use the frequency domain (FFT) for realizing the polyphase filters. This, together with the rate reduction due to the decimation in the filter bank, improves the computational burden, making real-time implementation of the high-order noise-canceling FIR filter practical. The sub-band filtering method provides *W(n)* of sufficiently high order to estimate *P(z)* and *S(z)* accurately. It also results in low computational delay compared to the acoustic delay, thus improving the stability of the ANC system.

The weight stacking block in Figure 2 computes the FFT of the weights of each LMS filter and puts these coefficients together in a special order to form the FFT of the coefficients of the final full band FIR filter *W(n)*. The time domain filter *W(n)* is then computed by the inverse FFT. This frequency-domain implementation of the sub-band filtering and stacking procedure was proposed by Morgan [6]. Method 1 in Section III describes the weight stacking procedure. The procedure acts as a synthesizing filter bank. As investigated in [7], the frequency response of these filters shows deep nulls in the pass-band, causing significant degradation in the system performance. The degradation reaches an unacceptable level in the case of fMRI acoustic noise, whose spectrum has strong tonal components. In contrast to Morgan's method, for the fMRI case, we have adapted the FFT-2 weight transform [7], which removes the nulls and results in a flatter frequency response over the pass-band than is achieved by Morgan's method. The adapted FFT-2 weight transform technique is presented as Method 2 in Section III. The frequency responses of the first sub-band (k=0) using the two methods are compared in Figure 5, where the removal of the pass-band nulls by the FFT-2 method can be seen.

## III. LMS-BASED ANC ALGORITHM USING SUB-BAND FILTERING

Let the filter bank in Figure 3 produces $M=2^n$ sub-band signals. The $k$'th analysis polyphase filter is

$$H_k(z) = \sum_{n=0}^{M-1} z^{-n} H_{k,n}(z^M) \tag{1}$$

$$X(z) = \sum_{n=0}^{M-1} z^{-M+n-1} X_n(z^M) \tag{2}$$

In vector, matrix notations, the polyphase components are:

$$\mathbf{H}_k(z) = [H_{k,0}(z), H_{k,1}(z), ..., H_{k,M-1}(z)]^T \tag{3}$$

$$\mathbf{X}(z) = [X_0(z), X_1(z), ..., X_{M-1}(z)]^T \tag{4}$$

$$\mathbf{Y}_k(z) = \mathbf{H}_k^T(z) \cdot \mathbf{X}(z) \tag{5}$$

Assume that the analysis filters are FIR with $L_p$ coefficients derived from a prototype filter $Q(z)$ by modulation. Thus,

$$\mathbf{h}_k = \underbrace{\begin{bmatrix} q[0] & & & 0 \\ & q[1] & & \\ & & \ddots & \\ 0 & & & q[L_p-1] \end{bmatrix}}_{\mathbf{Q}} \cdot \underbrace{\begin{bmatrix} t_k[0] \\ t_k[1] \\ \vdots \\ t_k[L_p-1] \end{bmatrix}}_{\mathbf{t}_k} \tag{6}$$

$$\mathbf{H}_k(z) = \underbrace{[\mathbf{I}_M \quad z^{-1}\mathbf{I}_M \quad \cdots \quad z^{-\lfloor L_p/M \rfloor}\mathbf{I}_M]}_{\mathbf{L}_1^T(z)} \cdot \mathbf{h}_k \tag{7}$$

We define $\mathbf{Q} \in R^{L_p \times L_p}$ as a diagonal matrix holding the prototype filter coefficients, and

$$\mathbf{t}_k = \underbrace{[\mathbf{I}_M \quad \mathbf{I}_M \quad \cdots \quad \mathbf{I}_M]^T}_{\mathbf{L}_2^T} \cdot \tilde{\mathbf{t}}_k \ , \ \mathbf{L}_2 \in N^{L_p \times M} \tag{8}$$

$$\mathbf{T} = [\tilde{\mathbf{t}}_0 \quad \cdots \quad \tilde{\mathbf{t}}_{M-1}]^T \in C^{M \times M} \tag{9}$$

Where $\mathbf{t}_k \in C^M$ is a $M \times 1$ complex vector. $\tilde{\mathbf{t}}_k$ ($k=0,\ldots, M-1$) stands for the modulation vector. For example, for a DFT modulated filter bank, the $\tilde{\mathbf{t}}_k$ would be the $k$th column of $M$-point DFT matrix:

$$\tilde{\mathbf{t}}_k(n) = e^{j\frac{2\pi}{M}kn}, \quad \text{for } n=0,\ldots,L_p-1 \tag{10}$$

Finally, the matrix notation for a polyphase analysis filter bank is [8]:

$$\mathbf{H}(z) = \mathbf{T} \cdot \mathbf{L}_2 \cdot \mathbf{Q} \cdot \mathbf{L}_1(z) \quad (11)$$

This filtering is applied to $x'(n)$, $e(n)$ as shown in Figure 2. The outputs are fed to LMS filters where the vectors of the filter coefficients $\boldsymbol{w}_i$ are computed for each sub-band. We then stack the weights similar to that of [6]. Assuming the lengths of $N$ and $L$ for the full-band noise-canceling filter $W(n)$ and every sub-band LMS filter respectively, the weight stacking is performed as follows:

*Method 1: Morgan's weight stacking procedure,* (12)

a) for $l \in [0, N/2)$,
$H(l) = H_{\lfloor lM/N \rfloor}((l)_{2N/M})$

b) for $l = N/2$, $H(N/2) = 0$

c) for $l \in (N/2, N)$, $H(l) = H(N-l)^*$

In the case of fMRI acoustic noise, we observe nulls in the frequency response at frequencies $(2l+1)\pi/N$ when the above method is used. To avoid the pass-band nulls, we replace the above method with the following FFT-2 weight-stacking method [7]:

*Method 2: FFT-2 weight stacking procedure,* (13)

a) for $l \in [0, N)$,
$H(l) = H_{\lfloor lM/2N \rfloor}((l)_{4N/M})$

b) for $l = N$, $H(N) = 0$

c) for $l \in (N, 2N)$, $H(l) = H(2N-l)^*$

Where $H(l)$ and $H_k(l)$ are the $l$th DFT coefficient of the full-band filter and the $k$th sub-band filter respectively. $\lfloor . \rfloor$ denotes rounding to the nearest integer and superscript * denotes complex conjugation.

## IV. SIMULATION RESULTS

Figure 1(a,b) shows the time and frequency domain representations of the recorded fMRI acoustic noise. Since FFT is used the order of $W(z)$ must be power of 2. Based on our simulation results performance of the system does not improve drastically for orders higher than 512 for $W(z)$. $P(z)$ and $S(z)$ were chosen to model the primary acoustic and the secondary paths respectively. So a full-band FIR filter of order 512 was realized using $M$ sub-bands to estimate $P(z)$ and $S(z)$. $P(z)$ and $S(z)$ were obtained experimentally for an actual acoustic cavity (a duct system) and the electronics path including the canceling load-speaker. They were non-minimum phase rational functions of order 25. Figure 6 shows the magnitude of the frequency response of the $P(z)$ and $S(z)$.

Table 1 shows the average noise reduction that was achieved versus the number of sub-bands used when $W(n)$ had 512 taps. For the fMRI acoustic noise, the best result in terms of SNR is obtained when 16 sub-band filters are used in Method 1 and 2. That is, the filter bank structure of 16 sub-band filters, each of length 32, produces the highest level of cancellation of the noise tonal components and its harmonics. The SNR is defined as the ratio of the actual fMRI noise power and the power of output error (i.e. the attenuated noise) in dB.

The performance comparison shown in Table 1 is based on using the two stacking methods described in Section III. Method 1 performs worse than method 2 due to the presence of the nulls in the pass-band. The SNR depends on both the positions of the nulls in the pass-band and the positions of tonal peaks in the noise spectrum. Increase in the number of sub-bands in method 1 increases the number of nulls in the pass-band, hence degrading the SNR. SNR also changes depending on the positions of the noise tonal peaks at the inputs of the sub-band filters. This effect manifests itself in having the best SNR for 16 sub-band filters. In method 2 the pass-band nulls are removed resulting in higher SNR than that for method 1 when the same number of sub-band filters is used.

In the LMS method where no sub-band filtering is used, all the 512 coefficients of the full-band filter must be updated for every input sample. In the sub-band method, we only need to update coefficients of the full-band filter $W(n)$ for every 8 samples of the input signal when 16 sub-bands are used. This in general reduces number of computations by a factor of about 3 (Table 2) over what is typically required for the full-band LMS method. Furthermore, the sub-band filtering could be implemented in parallel blocks, enabling real-time realization of this method.

Table 2 shows α as the ratio of computation time of the sub-band method over that of the full-band adaptive LMS filtering method. When the number of sub-bands increases the computational complexity ratio decreases exponentially. Our extensive simulations have shown that the number of sub-bands for obtaining maximum noise suppression depends on the spectrum characteristics of the noise signal. This number was shown to be 16 sub-bands for optimal suppression of the fMRI acoustic noise signal using the LMS-based methods presented in this paper. On the other hand using 32 sub-bands with the FFT-2 stacking method has nearly the same performance while its computational burden is almost half of the case when 16 bands are used.

## REFERENCES


[1] W. B. Edmister, T. M. Talavage, P. J. Ledden and R. M. Weisskoff, "Improved auditory cortex imaging using clustered volume acquisition," *Human Brain Mapping 7*, pp. 89-97, 1999.

[2] S. J. Elliot and P. A. Nelson, "Active noise control," *IEEE Signal Processing Magazine*, pp. 12-35, Oct. 1993.

[3] J Chambers, MA. Akeroyd, AQ Summerfield, and AR. Palmer, "Active control of the volume acquisition noise in functional magnetic resonance imaging: Method and psychoacoustical evaluation," *Journal of the Acoustical Society of America*, vol. 110, no. 6, pp. 3041–3054, December 2001.

[4] Nedelko Grbic, Jorgen Nordberg and Sven Nordholm, "subband acoustic echo canceling using LMS and RLS," Research report, May 1999.

[5] Sen M. kuo and Dennis R. Morgan, *Active Noise control Systems, algorithms and DSP implementations*, Wiley, US, 1996.

[6] Dennis R. Morgan and James C. Thi, "A Delayless subband adaptive filter architecture," IEEE transaction on signal processing, vol 43, No.8, pp.18-19-1830, August 1995.

[7] Jiaquan huo, Sven Nordholm and Zhuquan Zang, "New weight transform schemes for delayless subband adaptive filtering," Global Telecommunications Conference, GLOBECOM'01, vol.1, pp. 197 – 201, 2001.

[8] S. Weiss, "Analysis and Fast Implementation of Oversampled Modulated Filter Banks," In John G McWhirter and Ian K. Proudler (eds.): Mathematics in Signal Processing V, IMA, pp.263-274, 2001.

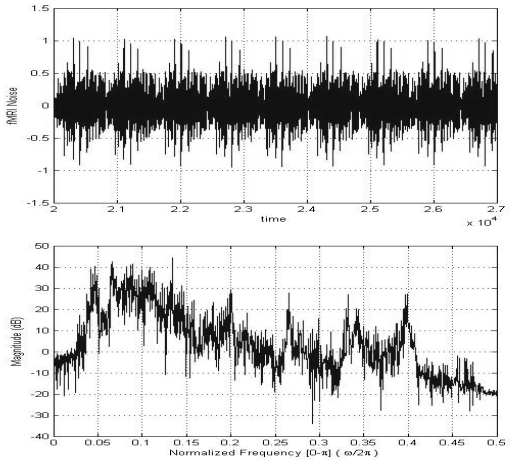


Fig.1.(a) fMRI noise (upper) and (b) fMRI noise spectrum (lower)

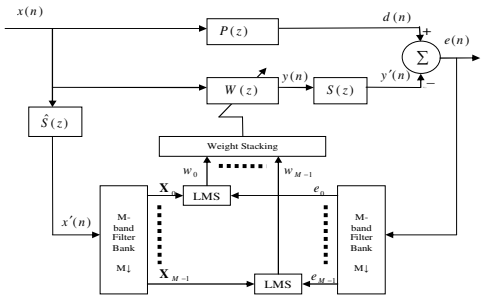


Fig. 2. Sub-band fMRI ANC

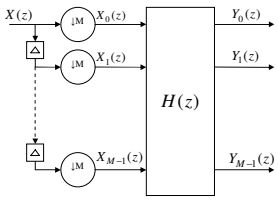


Fig. 3. Filter bank polyphase implementation

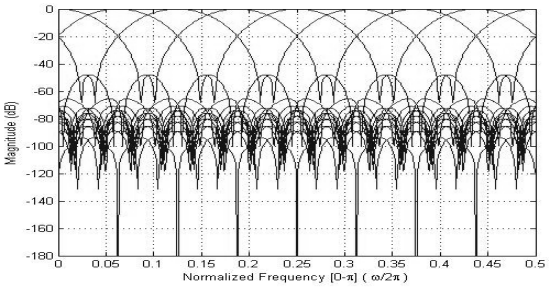


Fig. 4. Frequency response of filter bank, M=16

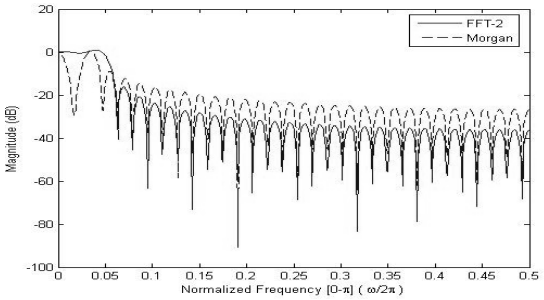


Fig. 5. The frequency response of FFT-2 (solid) and Morgan (dashed) for the first sub-band, k=0

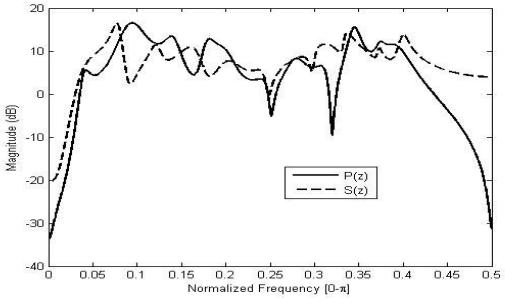


Fig. 6. Frequency response of the *P(z)* (solid) and *S(z)* (dashed)

Table 1. Average noise reduction for Method 1 and 2 over entire frequency range.

| # Sub-Bands | Noise Suppression (dB) Method 1 | Noise Suppression (dB) Method 2 |
|---|---|---|
| 1 (full-band ~512 tap) | 26.33 | 26.33 |
| 2 | 24.53 | 29.83 |
| 4 | 33.00 | 35.31 |
| 8 | 28.60 | 34.28 |
| 16* | 36.80* | 40.12* |
| 32 | 27.20 | 40.06 |

Table 2. α = (computation time using sub-band)/ (computation time using no sub-band)

| # of subbands → | 2 | 4 | 8 | 16 | 32 |
|---|---|---|---|---|---|
| α → | 2.3 | 1.59 | 0.64 | 0.31 | 0.17 |